



# Non-keyhole Friction Stir Welding for 6061-T6 Aluminum Alloy

Peng Gong<sup>1</sup> · Ying-Ying Zuo<sup>1</sup> · Shu-De Ji<sup>1</sup> · De-Jun Yan<sup>2</sup> · Deng-Chang Li<sup>1</sup> · Zhen Shang<sup>1</sup>

Received: 23 March 2021 / Revised: 30 April 2021 / Accepted: 19 May 2021 / Published online: 28 July 2021  
© The Chinese Society for Metals (CSM) and Springer-Verlag GmbH Germany, part of Springer Nature 2021

## Abstract

A novel non-keyhole friction stir welding technique was proposed to weld the butt joint of 6061-T6 aluminum alloy with the thickness of 6 mm. A sound joint was obtained by this technique, simultaneously eliminating the flash, shoulder mark and keyhole defects. The sleeve directly affected zone (SDAZ) and the sleeve indirectly affected zone (SIAZ) were divided into the joint according to the plunging position of the hollow sleeve. The lack of root penetration defect was avoided when the plunging depth of the hollow sleeve was only 4.2 mm, because the hollow part inside the sleeve improved the material flow below the sleeve. An S-shaped line was left at the SIAZ, and the height of it had the minimum value of 1.47 mm at 20 mm/min. Whether the failure location of the joint was in SIAZ/SDAZ or the heat-affected zone (HAZ) depended on the height and bonding strength of the S-shaped line. The joint fracture location changed from the SIAZ/SDAZ at 35 mm/min to the HAZ at 20 and 30 mm/min. The maximum tensile strength of 224.3 MPa was obtained at 30 mm/min which was 73.7% of that of the base material. The fracture surface morphology exhibited the typical ductile fracture.

**Keywords** Non-keyhole friction stir welding · Welding tool simplification · Microstructures · Material flow · Mechanical properties

## 1 Introduction

As a solid-state joining technique, the low heat input and strong mechanical stirring during welding are the main features of friction stir welding (FSW), and these features make FSW more promising in joining the low melting point metals like aluminum alloy [1, 2]. Due to the low heat input, the joint obtained by FSW has low residual deformation [3] and small heat-affected zone (HAZ) [4]. The strong mechanical stirring brings violent material flow, and sufficient material

flow is necessary for obtaining a high-quality joint for FSW [5, 6]. The tool pin plays a crucial role on material flow [7]. However, a keyhole inevitably remains at the end of joint with the tool pin retracting from the welded joint. The problem is that the keyhole not only affects the joint appearance, but also reduces the mechanical properties of the joint. The study of Rao et al. [8] showed that the fatigue life of weld with keyhole was much lower than that of the weld without keyhole. Moreover, the keyhole has another disadvantage of shortening the effective weld length.

Repairing the keyhole after welding is dominant in keyhole elimination. Zhou et al. [9] brought forward the self-refilling friction stir welding (SRFSW). Non-consumable tools with gradual change in geometry and the materials around the tools were used to refill the keyhole during SRFSW process. However, this method had the complex process and caused the thickness thinning of the repaired keyhole. In fact, in order to avoid the thickness thinning, the additional filling material (FM) is necessary. The friction plug welding (FPW) was proposed by Du et al. [10] to repair the keyhole using a consumable tool pin. However, the low heat input and poor material flow owing to the deformable rotational tool pin led to new defects such as cavities and kissing bond. Therefore, Huang et al. [11]

---

Ying-Ying Zuo and Peng Gong have been contributed equally to this work.

---

Available online at <http://link.springer.com/journal/40195>

✉ Shu-De Ji  
superjsd@163.com

✉ De-Jun Yan  
yandejun\_2003@163.com

<sup>1</sup> College of Aerospace Engineering, Shenyang Aerospace University, Shenyang 110136, China

<sup>2</sup> Guangdong Key Laboratory of Enterprise Advanced Welding Technology for Ships, CSSC Huangpu Wenchong Shipbuilding Company Limited, Guangzhou 510715, China

proposed filling friction stir welding (FFSW) and adopted a semi-consumable tool consisting of a non-consumable shoulder and consumable filling bit. More heat was generated because of the non-consumable shoulder, and a sound joint whose tensile strength (TS) was equal to 90% of the defect-free FSW weld. In addition, the drilling-filling friction stir repairing (D-FFSR) [12] was put forward to repair keyhole using a cylindrical FM and a pinless tool. Ji et al. [13] proposed the active–passive filling friction stir repairing (A-PFFSR) to repair the keyhole with a large depth by a series of pinless tools with different shoulder diameters. The keyhole can be well repaired after welding by the above-mentioned processes, but the repairing process after welding increases the process complexity, production time and cost. It is necessary to develop a technology which can eliminate the keyhole during the one-time welding process.

In this study, a novel non-keyhole FSW (N-KFSW) technology was proposed, which could eliminate the keyhole and obtain a smooth surface during the welding process. AA6061-T6 plates were chosen for N-KFSW experiments. Moreover, the surface appearances, microstructures and mechanical properties at different welding velocities were discussed.

## 2 Experimental

### 2.1 N-KFSW Process

The refilled friction stir spot welding (RFSSW) can get a non-keyhole welding spot [14, 15], and stationary shoulder

FSW (SSFSW) can improve the top surface quality of the joint [16]. The N-KFSW tool system has the structure similar as the tool system of RFSSW and possesses the advantages of RFSSW and SSFSW technologies. A non-keyhole joint with smooth surface can be obtained during N-KFSW process. The process of N-KFSW can be divided into three stages including the plunging, welding and refilling stages, as shown in Fig. 1. This N-KFSW tool system consists of an outer non-rotating clamping ring and an inner rotational sleeve and probe. At the plunging stage, the non-rotating clamping ring compresses the top surface of the plates tightly, the rotational sleeve plunges into the plates to be welded, and the rotational probe moves away from the top surface. A cavity is left between the sleeve and the probe at the plunging stage, and the cavity can collect the squeezed plasticized material [17]. The welding tool moves along the weld, and the volume of the cavity remains unchanged at the welding stage. At the refilling stage, the rotational sleeve moves upward while the rotational probe moves downward to refill the keyhole due to the upward movement of the sleeve. At the same time, the rotational sleeve and probe stay some seconds to get a good formation before the welding tool retracts from the welded plate. During N-KFSW process, the clamping ring has the sealing and extra-forging effects and the rotational sleeve provides the major heat, and the rotational sleeve and probe can drive the plasticized material to flow.

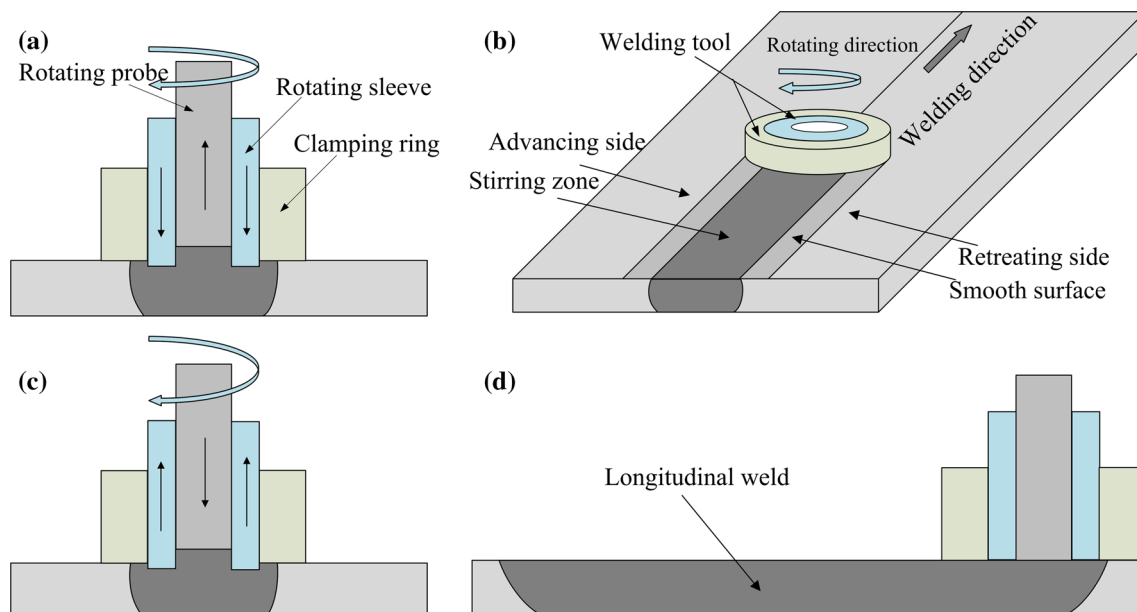


**Fig. 1** Schematic diagram of N-KFSW process: **a** plunging stage, **b** welding stage, **c** refilling stage, **d** after welding

## 2.2 Simplification of Welding Tool

The N-KFSW tool system was designed by AVIC Manufacturing Technology Institute. The outer diameters of the probe, sleeve and clamping ring were 6, 9 and 18 mm, respectively, as shown in Fig. 2a. Both probe and sleeve had the left-hand thread which had 1.5 mm pitch and 0.2 mm depth. For the sleeve, the ending point of thread was 1 mm away from the top surface of the sleeve. During the welding process, the coordination among different parts was complex, and the cost was expensive. Importantly, the N-KFSW tool system, especially the sleeve, was easy to wear and even break [18]. Therefore, a simplified hollow tool (SHT) which had the same effect as the N-KFSW tool was designed (Fig. 2b). The SHT consisted of two parts including a hollow sleeve (sleeve with a blind hole) and a clamping ring. In fact, the clamping ring of the SHT played the roles of sealing and extra-forging and the hollow sleeve provided the heat and stirring effects. In addition, this hollow part was regarded as the safe space left and it had the same diameter with the probe. The hollow part had the height of 9 mm, which was the biggest distance between the top surfaces of the sleeve and the probe during welding when the N-KFSW tool system was used. The SHT has a different appearance from the N-KFSW tool and the specific dimensions of the SHT are described as follows.

The hollow sleeve had an outer diameter of 9 mm. The diameter and depth of the hollow part were 6 and 9 mm, respectively. A left-hand thread with 1.5 mm pitch and 0.2 mm thread depth was equipped with the outer surface of the hollow sleeve. The ending point of thread on the outer wall of sleeve was also 1 mm away from the top surface of the hollow sleeve. The clamping ring had the outer diameter of 18 mm and inner diameter of 9 mm. The welding schematic using the SHT is shown in Fig. 2c. Preliminary N-KFSW experiments were performed, and a non-keyhole joint with smooth surface was obtained when the rotational and welding velocities were 1200 rpm and 20 mm/min.

According to these research results, the rotational velocity was the constant of 1200 rpm, and the welding velocities of 20 mm/min, 30 mm/min, 35 mm/min and 40 mm/min were selected in the experiment for attaining the higher welding efficiency. The plunging depths of the hollow sleeve and the clamping ring were 4 mm and 0.2 mm, respectively, and the tool-tilting angle was  $2.0^\circ$ . The rotational hollow sleeve was chosen to rotate clockwise according to the thread morphology.

## 2.3 Experimental Materials and Characterization

The aluminum alloy plates of 6061-T6 with the dimensions of 200 mm  $\times$  120 mm  $\times$  6 mm were chosen in the experiment. After welding, the metallographic and the tensile specimens (Fig. 3) were cut by a wire-cutting machine, and the cutting direction was perpendicular to the welding direction. The microstructure was etched by the Keller's reagent. The joint cross sections and microstructures were observed by the optimal microscopy (OM). The tensile tests were performed at the loading speed of 2 mm/min under room temperature, and there were three tensile specimens at each set of process parameters. The fracture paths and fracture surfaces were observed by the OM and the scanning electron microscopy (SEM), respectively. The microhardness was measured at the load of 300 g for 10 s.

## 3 Results and Discussion

### 3.1 Surface Morphologies

The joint surface appearances at different welding velocities are displayed in Fig. 4. The flash, shoulder mark and groove are the main defects which appear at the joint surface. The plasticized materials are squeezed out of the weld by the welding tool during the welding stage, which leads to the flash on the joint top surface and causes material loss of the

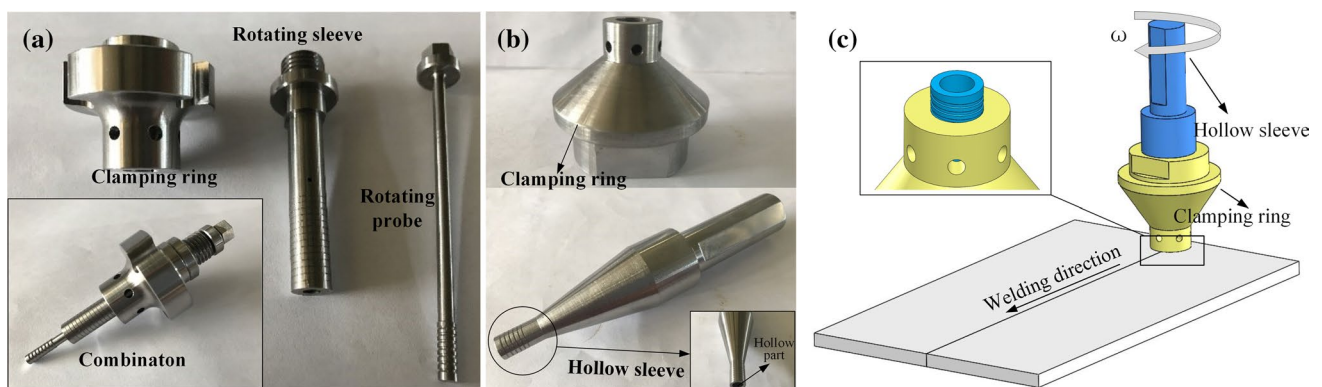


Fig. 2 a N-KFSW tool system, b SHT system, c welding schematic using the SHT

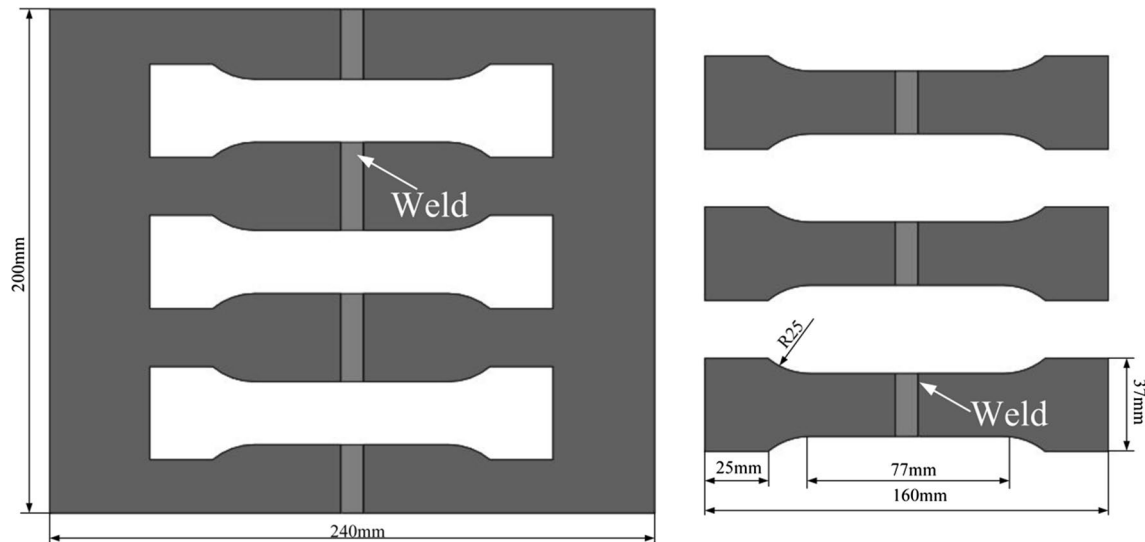


Fig. 3 Schematic of tensile specimens

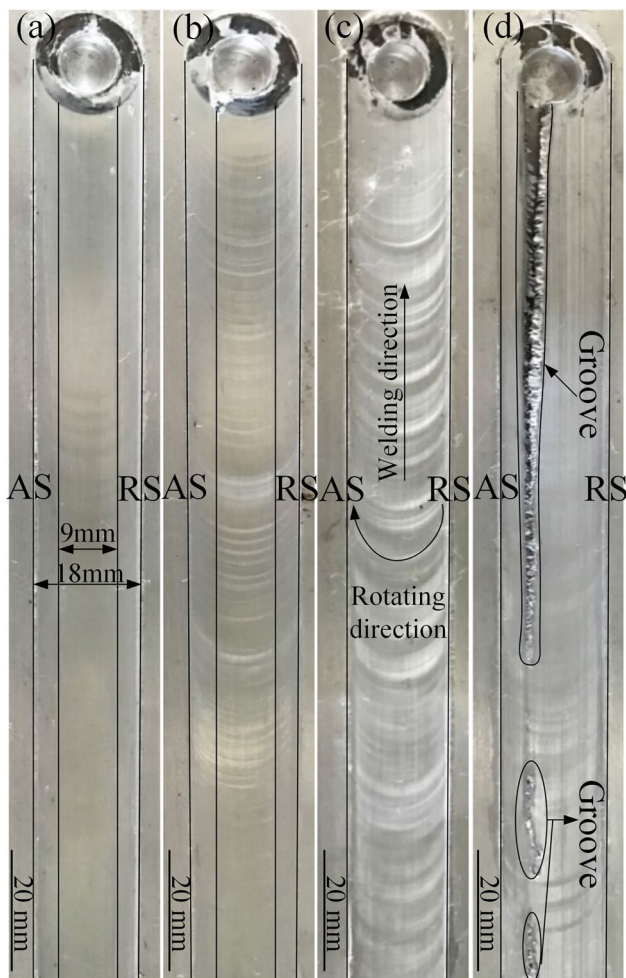


Fig. 4 Surface morphologies at different welding velocities: **a** 20 mm/min, **b** 30 mm/min, **c** 35 mm/min, **d** 40 mm/min

weld [19]. Moreover, the groove is easily formed at the joint surface when the materials which flow into the advancing side (AS) from the retracting side (RS) are not enough. In brief, poor material flow and a large amount of material loss are mainly responsible for the groove defects in the joint. Li et al. [19] pointed out that the sealing effect of stationary shoulder prevented the material from flowing out of the weld, which was beneficial to eliminating flash and then remaining more material in the weld. It can be seen that the non-rotating clamping ring of the SHT system owns the sealing effect. Therefore, a smooth surface without any obvious surface defects in the joint surface was obtained, as shown in Fig. 4a. However, at the higher welding velocity of 40 mm/min, the material has a poor flow behavior due to the lower heat input and worse stirring effect per unit length, so a long groove occurs on the top surface of the joint.

### 3.2 Cross Sections

The cross sections of joints at 20, 30 and 35 mm/min are displayed in Fig. 5. The cross section can be divided into sleeve directly affected zone (SDAZ), sleeve indirectly affected zone (SIAZ), thermal-mechanical affected zone (TMAZ), HAZ and based material (BM). The final position of the top surface of the hollow sleeve is regarded as the borderline between the SDAZ and the SIAZ. The SDAZ has a drum-like shape and the onion ring structure is formed here. The widths of the SDAZ top surface (line 1) and the widths which were 4 mm (line 2) away from the joint bottom surface at different welding velocities were measured. The measured widths all decrease when the welding velocities increase to 40 mm/min from 20 mm/min, and the maximum values are 9.8 and 10.6 mm at 20 mm/min, respectively. Moreover,



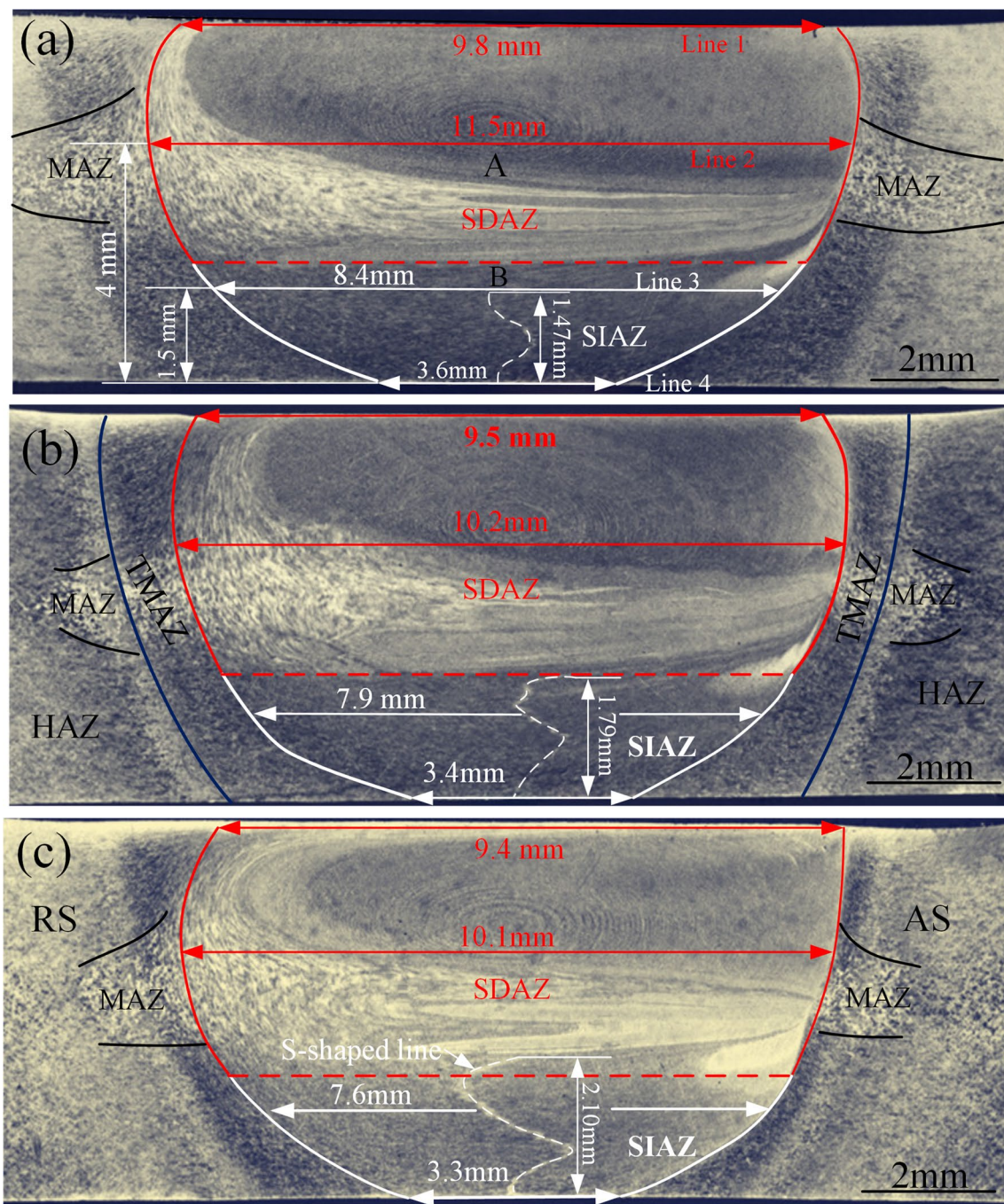


Fig. 5 Cross sections at different welding velocities: a 20 mm/min, b 30 mm/min, c 35 mm/min

the clamping ring not only absorbs the heat of material [15, 19] but also constrains the flow of material contacting the clamping ring, which has a negative effect on the material flow. Thus, the top area of the SDAZ has a smaller width than the middle area. According to the material flow analysis of the conventional solid pin with the thread [20], the materials around the outer wall of the hollow sleeve flow down along the thread and then release at the ending point

position of the thread. Hence, an obvious material accumulated zone (MAZ) is formed at the bottom of SDAZ, and it is at a distance from the borderline between the SDAZ and the SIAZ. In addition, the MAZ which is located in the RS is bigger than that in the AS. This is because more materials are directly deposited at the RS when the materials in front of the hollow sleeve flow into the rear of the sleeve through the RS. There is a strong material flow in the SDAZ and the



dynamic recrystallization happens in the SDAZ under the high welding temperature, so the butt interface in SDAZ is invisible.

The SIAZ has a bowl-like shape. The widths of the SIAZ which were 1.5 mm (line 3) and 0 mm (line 4) away from the joint bottom surface at different welding velocities were measured. As the distance from the top surface of the hollow sleeve increases, the heating and stirring effects of the sleeve are weakened sharply, so the width difference between the lines 3 and 4 in the SIAZ is more than 4 mm. Of course, the widths of the SIAZ also decrease as the welding velocity increases. Under conventional FSW, the distance between the top surface of conventional solid pin and the bottom surface of joint is commonly no more than 0.2 mm for avoiding the lack of root penetration defect [21, 22]. However, the distance between the top surface of hollow sleeve and the joint bottom surface is 1.8 mm and there is no lack of root penetration defect in this study. This phenomenon can be attributed to the improved material flow caused by the hollow sleeve.

The lack of root penetration defect is avoided when the plunging depth is only 4.2 mm but the thickness of BM is 6 mm owing to the improved material flow. However, the thermal cycle and the stirring effect in the SIAZ are much lower compared with those in the SDAZ, which causes that the butt interface is slightly transferred. Therefore, the butt interface exists as an S-shaped white line in SIAZ, which can be observed in the OM image. The temperature and the stirring effects decrease as the welding velocity increases from 20 mm/min to 35 mm/min, and then, the material flow is weakened, so the height of the S-shaped line increases from 1.47 mm to 2.13 mm. In addition, the local S-shaped line can be found in the bottom of SDAZ at 35 mm/min. For the S-shaped line, the bonding mechanism is the atom diffusion and then the corresponding bonding strength is relatively low, so the increase of S-shaped line height is detrimental to the carrying capacity of welding joint, which is further explained by the tensile experimental results in the following part.

### 3.3 Microstructures Analysis

The typical microstructures of the joint at 20 mm/min are analyzed and displayed in Fig. 6. Figure 6a shows the TMAZ at AS of the joint. The grains in TMAZ are broken and distorted because they undergo the severe deformation, and a clear boundary exists between the TMAZ and SDAZ. Microstructures of TMAZ can directly reflect the vertical material flow behaviors where far away from the hollow sleeve. Therefore, the materials in TMAZ present an upward flowing morphology (Fig. 6a) because of the driving effect by the MAZ. The HAZ only experiences a lower thermal cycle and the grain grows, so the grain in HAZ (Fig. 6b) is bigger than that in BM (Fig. 6c). There are black particles with the long-strip or round shape in different zone of the joint, and they are the dispersed precipitate. The size of precipitates in HAZ is the maximum because the precipitates are coarsened under the thermal cycle during welding.

The magnified microstructures of SDAZ and SIAZ are shown in Fig. 7. Area A is located in the middle of the SDAZ, and area B is at the top of the SIAZ. The SDAZ experiences the highest temperature cycle and the strongest stirring because of the direct effect of the hollow sleeve. Hence, the SDAZ consists of the fine equiaxed grains owing to the dynamic recrystallization, as displayed in Fig. 7a. The SIAZ also experiences the dynamic recrystallization. However, the thermal cycle in SIAZ is lower than that in SDAZ, so the grain-growth is smaller during the recrystallization process, causing that the grain size in area B (Fig. 7b) is smaller than that in area A. At the same time, the fine particles are uniformly distributed in the SDAZ and SIAZ.

According to the cross sections and the microstructures, the schematic of material flow around the hollow sleeve during the welding process is displayed in Fig. 8. The material flow around the outer surface of the hollow sleeve has the same regularity with the traditional solid pin with thread [20, 23, 24]. The materials in the hollow part flow to the inner wall of the hollow sleeve under the centrifugal force and then flow downward after contacting with the inner wall.

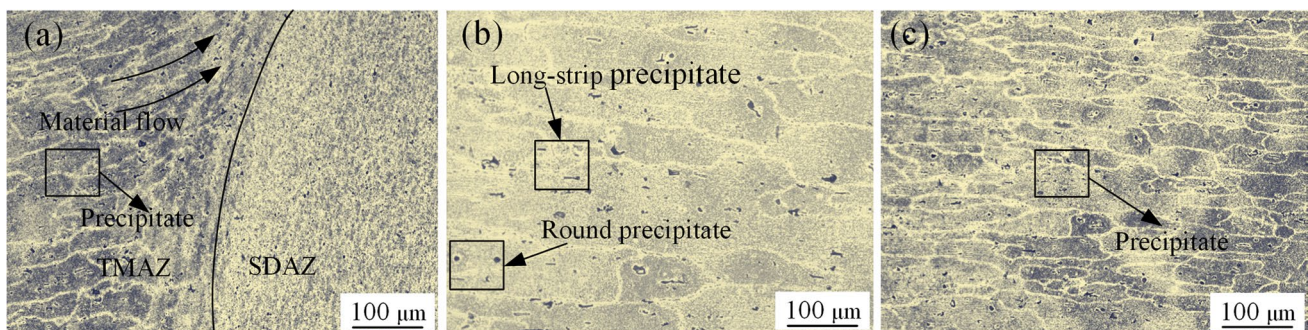


**Fig. 6** Microstructures of typical zones: **a** TMAZ, **b** HAZ, **c** BM

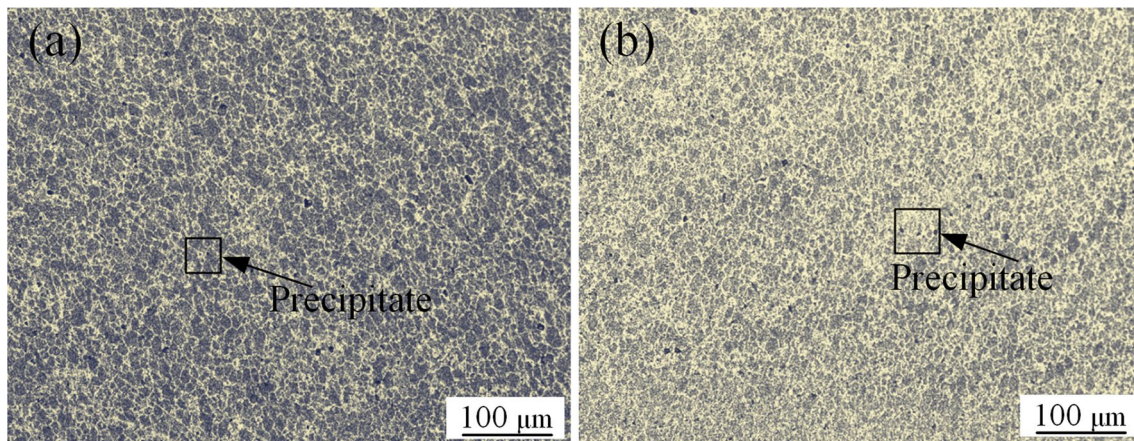


Fig. 7 Magnified microstructures of SDAZ and SIAZ marked in Fig. 3a: **a** area A, **b** area B

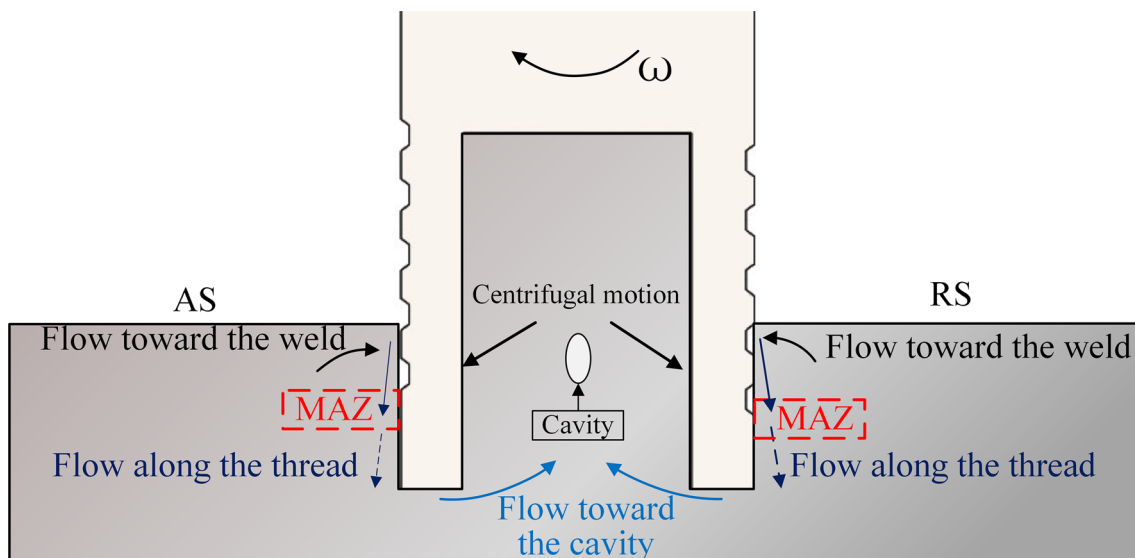


Fig. 8 Schematic of material flow under the hollow sleeve

Therefore, the materials in the center of the hollow part are sparse and the cavity is formed here, as reported by Ji et al. [25] and Cao et al. [26]. According to the law of minimum resistance, the materials under the sleeve are forced to flow into the hollow part for filling the cavity [27]. Finally, the materials between the hollow part and below the sleeve form a new flow path, which means the hollow part promotes the material flow below the sleeve.

### 3.4 Microhardness

The microhardness values of line 2 and line 3 marked in Fig. 5a were measured. The measured lines 2 and 3 are 2 and 4.5 mm away from the top surface of the joint and located in SDAZ and SIAZ, respectively. In addition, the spacing

between two adjacent points was 0.5 mm. The microhardness distributions at the welding velocity of 20 mm/min are displayed in Fig. 9. The microhardness values parallel to the joint top surface are distributed in a "W" shape. Fine grain strengthening and precipitation hardening are the main strengthening mechanisms of 6061 aluminum alloy [28]. The fine equiaxed grains and the homogeneous distributed fine precipitation phase can increase the microhardness value in SDAZ and SIAZ. However, the dissolution or partial dissolution of hardening precipitates in the SDAZ and SIAZ during the elevated temperature has the adverse impact on the microhardness values [29], so the microhardness in SDAZ (about 72HV) and SIAZ (about 82 HV) is lower than the microhardness in BM (about 95 HV). The grain in SIAZ is smaller than that in SDAZ (Fig. 9), so the



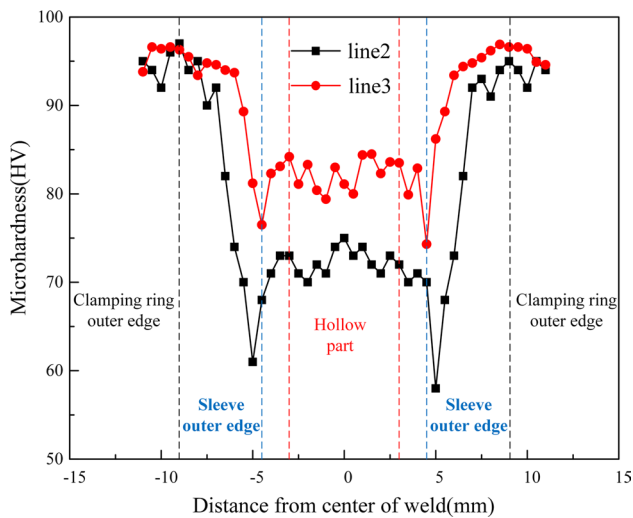


Fig. 9 Microhardness testing results at 20 mm/min

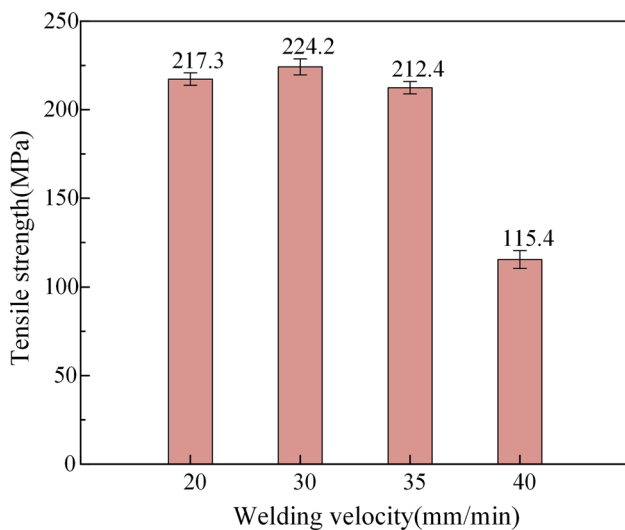


Fig. 10 Tensile strength test results

microhardness value in SIAZ is bigger than that in SDAZ. In HAZ, both the coarsening of the  $Mg_2Si$  precipitates and the grain size play the major roles in the microhardness, so the induced minimum microhardness (57 HV) is only about 60% of the BM. Local dynamic recrystallization and dislocation strengthening make the microhardness in TMAZ higher than that in HAZ.

### 3.5 Tensile Strength

Figure 10 shows the TS values at different welding velocities. The TS increases first and then decreases with the increase in welding velocity. Furthermore, the maximum TS of 224.3 MPa is acquired at 30 mm/min and the value

reaches 73.7% of that of BM (304 MPa). The minimum TS of 115.4 MPa is obtained at 40 mm/min, which is only 38% of that of BM, and the groove shown in Fig. 4d is mainly responsible for the minimum strength of the joint. The TS increases by 6.9 MPa as the welding velocity changes to 30 mm/min from 20 mm/min. As mentioned above, the increase in S-shaped line height is detrimental to the carrying capacity of welding joint. Although the height of the S-shaped line at 30 mm/min is 0.32 mm larger than that at 20 mm/min, the TS is still promoted. This proves that the material softening in reducing tensile properties plays the dominant effect in this parameter range. Moreover, the TS is dominated by the S-shaped line when the welding velocity changes from 30 mm/min to 35 mm/min.

### 3.6 Fracture Behavior

The fracture locations of the joint produced at different welding velocities are displayed in Fig. 11. Two types of fracture modes have been identified. For the first mode, the failure location is in the HAZ, as shown in Fig. 11a, b. The second failure mode is that the fracture path is located in the SDAZ/SIAZ, as shown in Fig. 11c. The yield strength of the material is inversely proportional to the average grain size, and the coarser the average grain size, the lower the material yield strength. The HAZ has the largest grains (Figs. 6, 9), so the joint easily fails here due to the corresponding lowest carrying capacity. As mentioned above, the bonding strength of the S-shaped line at SIAZ is determined by atom diffusion, and the diffusion is influenced by the temperature and material flow. The higher heat input and the stronger material flow can promote the atom diffusion of the S-shaped line, thereby improving the strength of the joint. A stronger bonding of S-shaped line is formed at 20 mm/min and 30 mm/min, so the HAZ with the lowest microhardness value becomes the weakest zone and the joint fracture at the HAZ at AS. Under the action of tensile force, the local necking can be observed at the joint. The necking occurs at the HAZ in Fig. 11a, b, and the degree of the necking is more obvious at 30 mm/min. Moreover, the bottom part of S-shaped line at 20 mm/min appears crack owing to the material softening at the elevated temperature. At the welding velocity of 35 mm/min, the S-shaped line becomes the weakest zone which is accountable to the poor atomic diffusion, so the joint fractures from the S-shaped line and then spreads at the SDAZ. In addition, the obvious necking is observed at the SDAZ. From the results in Figs. 10 and 11, it is concluded that the S-shaped line is one of the major factors to determine the tensile strength and the failure mode of the N-KFSW joints.

Figure 12 shows the SEM images of fracture surface at 20 mm/min and 35 mm/min. The different locations of the fracture surfaces show the ductile fracture mode with



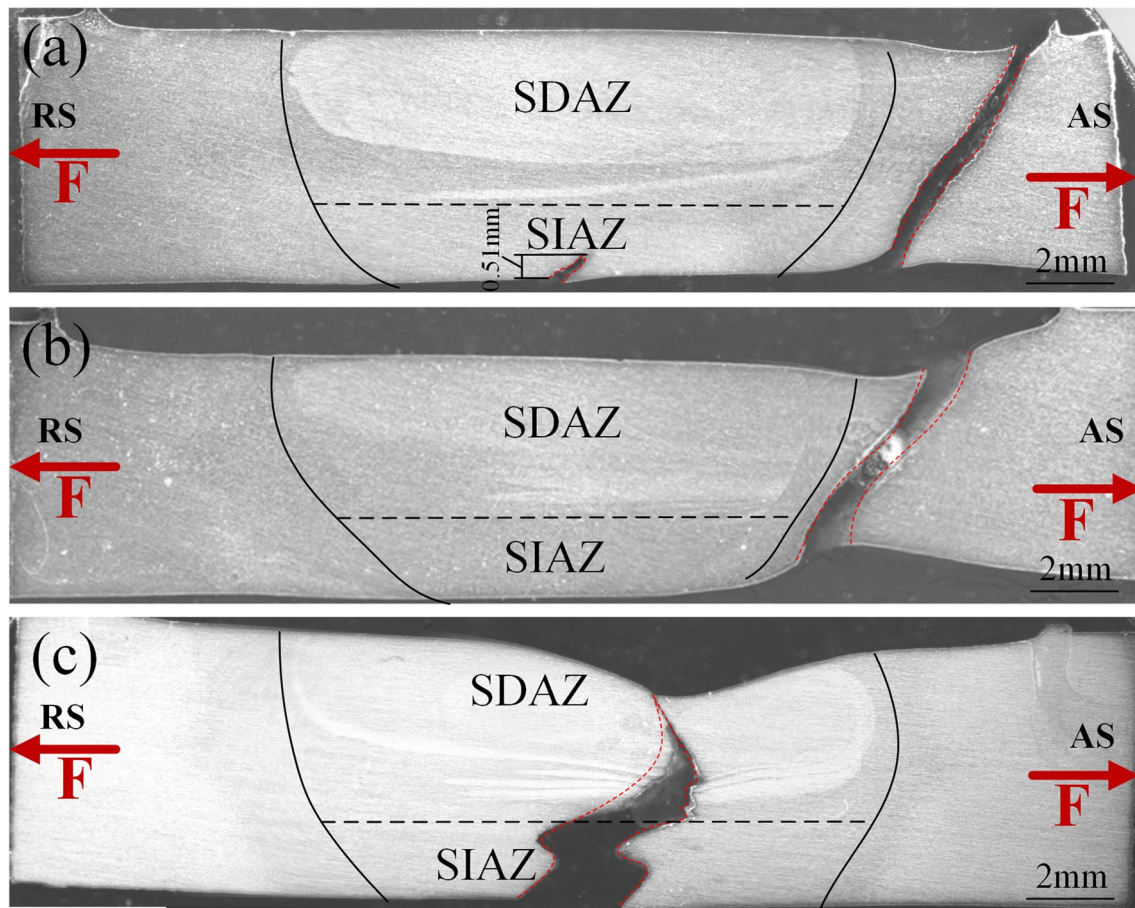


Fig. 11 Failure modes at a 20 mm/min, b 30 mm/min, c 35 mm/min

dimples. The appearance of the big and deep dimples is due to the large number of crystalline phases. The grain size in HAZ is much bigger than that in SDAZ and SIAZ, as shown in Figs. 5 and 6, so the dimples in HAZ (Fig. 12a, b) are larger than those in SDAZ (Fig. 12c) and SIAZ (Fig. 12d). The dimples with the small size are also found because of the precipitation phase in HAZ, SDAZ and SIAZ (Figs. 5, 6), and the small dimples are located inside or between the larger dimples. Moreover, when the welding velocity is 35 mm/min, the dimples in Fig. 12c are shallower and sparser compared with those in Fig. 12d because of the poor atom diffusion of S-shaped line.

#### 4 Conclusions

The 6061-T6 aluminum alloy plate with 6 mm thickness was welded by the N-KFSW technique. The surface formations, microstructures and mechanical properties at different welding velocities were analyzed in this study. The following conclusions were obtained:

1. The joint without flash and shoulder mark was obtained at the welding velocity of 20 mm/min. The lack of root penetration was avoided when the distance between the top surface of hollow sleeve and the bottom surface of joint was 1.8 mm owing to the hollow part in the sleeve.
2. The S-shaped line was formed because the butt interface was transferred. The height of S-shaped line increased with the welding velocity increasing and the value arrived the minimum value of 1.47 mm at 20 mm/min. The height and the bonding strength of S-shaped line determined the tensile strength and failure mode of the joint.
3. The maximum tensile strength was 224.3 MPa at 30 mm/min. The failure location was at the SIAZ/SDAZ under the high welding velocity, while the failure location was located in the HAZ under low welding velocity. The fracture surfaces all showed the ductile fracture mode with dimples.

**Acknowledgements** This work was financially supported by the National Natural Science Foundation of China (No. 51874201), the Guangdong Special Branch Plans (No. 2019TQ05C752) and the Education Department Foundation of Liaoning Province (No. JYT2020051).

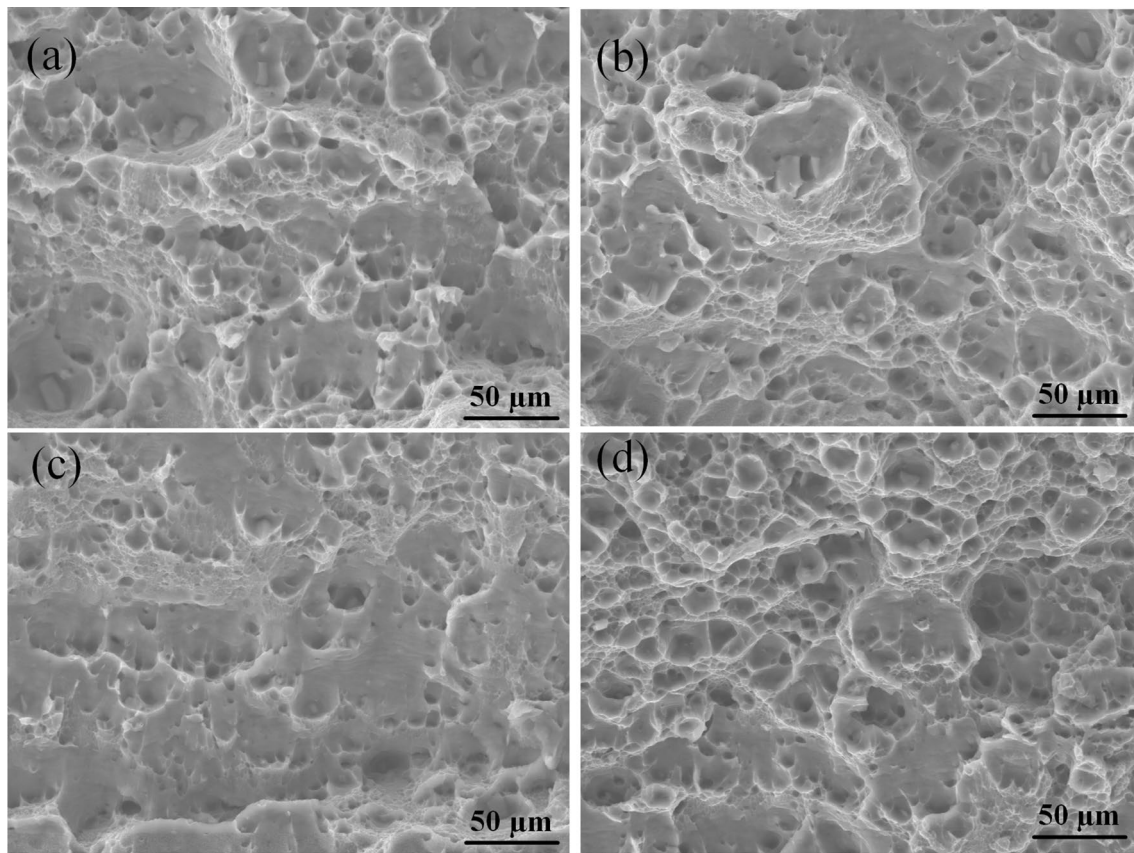


**Fig.12** Fracture surface micrographs at typical areas: **a** middle area and **b** bottom area in HAZ at 20 mm/min; **c** SIAZ, **d** SDAZ at 35 mm/min

## References

- [1] X. Meng, Y. Huang, J. Cao, J. Shen, J.F. dos Santos, *Prog. Mater. Sci.* **115**, 100706 (2021)
- [2] P. Yu, C.S. Wu, L. Shi, *Acta Mater.* **207**, 116692 (2020)
- [3] W. He, J. Liu, W. Hu, G. Wang, W. Chen, *High Temp. Mater. Process.* **38**, 662 (2019)
- [4] R. Nandan, T. Debroy, H. Bhadeshia, *Prog. Mater. Sci.* **53**, 980 (2008)
- [5] B. He, L. Cui, D. Wang, H. Li, C. Liu, *Acta. Metall. Sin.-Engl. Lett.* **33**, 137 (2020)
- [6] S. Ji, Q. Wen, Z. Li, *J. Mech. Sci. Technol.* **48**, 23 (2020)
- [7] Y. Huang, Y. Wang, L. Wan, H. Liu, J. Shen, J.F. dos Santos, L. Zhou, *J. Feng, Int. J. Adv. Manuf. Technol.* **87**, 1115 (2016)
- [8] H. Rao, J. Jordon, S. Boorgu, H. Kang, W. Yuan, X. Su, *Int. J. Fatigue* **105**, 16 (2017)
- [9] S. Ji, X. Meng, Y. Zeng, L. Ma, S. Gao, *Mater. Des.* **97**, 175 (2016)
- [10] B. Du, X. Yang, K. Liu, Z. Sun, D. Wang, *Weld. World.* **63**, 989 (2019)
- [11] Y. Huang, B. Han, S. Lü, J. Feng, X. Chen, *Trans. China Weld. Inst.* **33**, 5 (2012)
- [12] R. Huang, S. Ji, X. Meng, Z. Li, *J. Mater. Process. Technol.* **255**, 765 (2018)
- [13] L. Zhou, D. Liu, K. Nakata, T. Tsumura, H. Fujii, K. Ikeuchi, Y. Michishita, Y. Fujiya, M. Morimoto, *Sci. Technol. Join.* **17**, 649 (2013)
- [14] Y. Wang, P. Chai, H. Ma, X. Cao, Y. Zhang, *J. Mater. Sci.* **55**, 358 (2020)
- [15] G. Sun, L. Zhou, R. Zhang, L. Luo, H. Xu, H. Zhao, N. Guo, D. Zhang, *Acta. Metall. Sin.-Engl. Lett.* **33**, 551 (2020)
- [16] H. Wu, Y. Chen, D. Strong, P. Prangnell, *J. Mater. Process. Technol.* **221**, 187 (2015)
- [17] M. Reimann, J. Goebel, J. Dos Santos, *Mater. Des.* **132**, 283 (2017)
- [18] T. Montag, J. Wulfsberg, H. Hameister, R. Marschner, *Proced. CIRP* **24**, 108 (2014)
- [19] W. Li, P. Niu, S. Yana, V. Patel, Q. Wen, *J. Manuf. Process.* **34**, 159 (2019)
- [20] S. Ji, Z. Li, Z. Zhou, B. Wu, *J. Mater. Eng. Perform.* **26**, 5085 (2017)
- [21] G. Cam, S. Gueglueer, A. Cakan, H. Serindag, *Materialwiss. Werkst.* **40**, 638 (2010)
- [22] J. Li, Z. Sun, C. Gao, C. Dong, G. Luan, *Electric Weld. Mach.* **44**, 18 (2014)
- [23] L. Shah, A. Midawi, S. Walbridge, A. Gerlich, *J. Alloys Compd.* **826**, 154219 (2020)
- [24] Y. Yue, Z. Zhou, S. Ji, L. Zhang, Z. Li, *Int. J. Adv. Manuf. Technol.* **90**, 2597 (2016)
- [25] S. Ji, Z. Li, Y. Wang, L. Ma, L. Zhang, *High Temp. Mater. P-us.* **36**, 495 (2016)
- [26] J. Cao, M. Wang, L. Kong, Y. Yin, L. Guo, *Int. J. Adv. Manuf. Technol.* **89**, 2129 (2017)
- [27] G. Li, L. Zhou, L. Luo, X. Wu, N. Guo, *Int. J. Min. Met. Mater.* **28**, 131 (2021)
- [28] L. Zhang, H. Zhong, S. Li, H. Zhao, J. Chen, L. Qi, *Int. J. Fatigue* **135**, 1056 (2020)
- [29] M. Abdulstaar, K. Al-Fadhalah, L. Wagner, *Mater. Character.* **126**, 64 (2017)